Strongly Confined Excitons in GaN/AlN Nanostructures with Atomically Thin GaN Layers for Efficient Light Emission in Deep-Ultraviolet

A.A. Toropov, E.A Evropeitsev, M. O. Nestoklon, D.S. Smirnov, T. Shubina,
V.Kh. Kaibyshev, G.V. Budkin, V.N. V. N. Jmerik, D.V. Nechaev, S.
Rouvimov, et al.

Strongly Confined Excitons in GaN/AlN Nanostructures with Atomically Thin GaN Layers for Efficient Light Emission in Deep-Ultraviolet

A. A. Toropov,*[†] E. A. Evropeitsev,[†] M. O. Nestoklon,[†] D. S. Smirnov,[†] T. V. Shubina,[†]
V. Kh. Kaibyshev,[†] G. V. Budkin,[†] V. N. Jmerik,[†] D. V. Nechaev,[†] S. Rouvimov,[‡] S. V. Ivanov,[†]
and B. Gil[†,§]

[†]Ioffe Institute, St. Petersburg 194021, Russia

[‡]University of Notre Dame, Notre Dame, Indiana 46556, United States

[§]Université Montpellier, L2C, UMR 5221, 34095 Cedex 5 Montpellier, France

ABSTRACT: Fascinating optical properties governed by extremely confined excitons have been so far observed in 2D crystals like monolayers of transition metal dichalcogenides. These materials, however, are limited for production by epitaxial methods. Besides, they are not suitable for the development of optoelectronics for the challenging deep-ultraviolet spectral range. Here, we present a single monolayer of GaN in AlN as a heterostructure fabricated by molecular beam epitaxy, which provides extreme 2D confinement of excitons, being ideally suited for light generation in the deep-ultraviolet. Optical studies in the samples, supplemented by a group-theory analysis and first-principle calculations, make evident a giant enhancement of the splitting between the dark and bright excitons due to short-range electron−hole exchange interaction that is a fingerprint of the strongly confined excitons. The practical significance of our results is in the observation of the internal quantum yield of the room-temperature excitonic emission as high as ∼75% at 235 nm.

KEYWORDS: Excitons, 2D nanostructures, gallium nitride, photoluminescence, DFT calculation
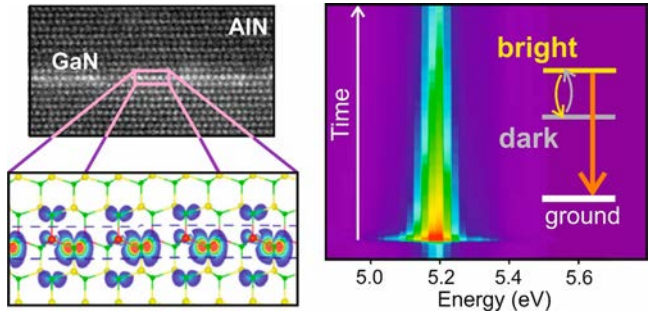
A distinctive feature of two-dimensional (2D) semiconductor structures is the significantly enhanced Coulomb interaction of electrons and holes, drastically increasing both exciton binding energy and oscillator strength.[1] The strongly confined excitons can be advantageous for efficient light generation due to the enhanced rate of the excitonic transitions, which allows one to improve trade-off between radiative and nonradiative recombination channels and, hence, to increase the emission quantum yield.[2,3] In the past years, most of the efforts toward realization of the extreme 2D confinement have been focused on 2D crystals like single monolayers (MLs) of transition metal dichalcogenides (TMDs), which possess the exciton binding energy as large as several hundreds of meV that gives rise to the existence of the tightly bound 2D excitons up to room temperature.[4,5] At low temperatures, the intrinsic radiative lifetime in these structures is an order of magnitude shorter than in conventional III−V quantum wells (QWs),[3,5] and one can imagine that the enhanced rate of the excitonic transitions might be a valuable resource for improving the device characteristics. For room temperature, this approach is, unfortunately, not straightforward, since the effective exciton radiative decay rate is given by an average over the thermal distribution among all excitonic states, including states with the large wavevectors outside the light cone, which are optically dark.[6] The width of the "radiative window" (E_0) including the excitonic states with their wavevectors within the light cone in the state-of-the-art TMD systems is rather narrow. As a result, the exciton radiative lifetime at room temperature is usually long enough, and nonradiative decay channels dominate over the radiative ones, making the light emission inefficient.

This obstacle could be overcome in 2D nanostructures of wide-band-gap semiconductors, like GaN and AlN, because the E_0 value is proportional to the squared exciton transition energy. Figure 1 shows the comparison between the widths of the radiative windows in a GaN/AlN ML and an ML of MoSe$_2$. The material parameters are taken from ref 7 for the GaN/AlN structure and from ref 8 for the TMD one. Obviously, E_0 can be an order of magnitude larger in the GaN ML than in the typical TMD 2D crystal (see the Supporting Information (SI) for the calculation details). Therefore, we
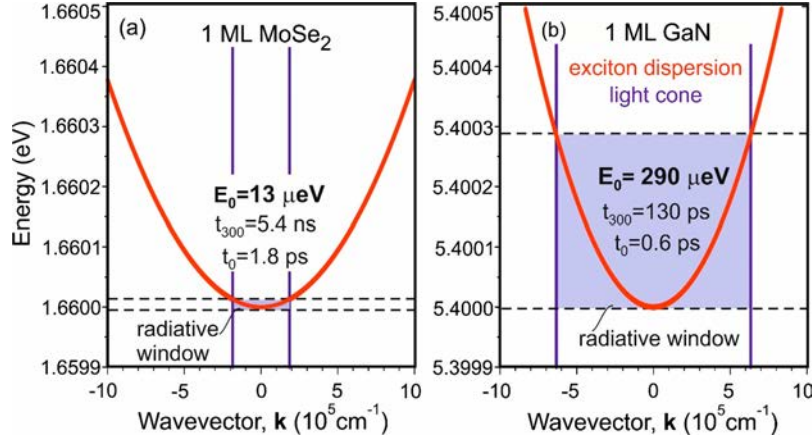
Figure 1. Scheme of the lowest-energy bright exciton dispersion and the light cone (vertical straight lines in this scale) in the exciton zone center for (a) a MoSe$_2$ ML and (b) a hypothetical 2D structure with the parameters of GaN and the exciton transition energy equal to 5.4 eV. Filled areas in the figures mark the radiative windows. The scales in two plots are the same, apart from the vertical offset of the excitonic levels for the possibility to compare.

assume that the GaN/AlN ML might be the most appropriate nanostructures for designing efficient room-temperature excitonic emitters, which is especially welcome for the yet poorly developed deep-UV optoelectronics. Among the most important problems of deep-UV emitters based on III-nitride compounds, which have a pyroelectric wurtzite crystal structure, are the huge dislocation density in the structures grown on non-native substrates as well as spontaneous and piezoelectric polarization-induced internal electric fields in the active regions.[9−13] These factors are responsible for accelerated nonradiative recombination and suppressed radiative recombination that results in the decreased internal emission efficiency. The increased rate of excitonic transitions in GaN QWs of ultimate thickness and very high quality should improve the situation, increasing the emission quantum yield.

The GaN/AlN QWs are the nanostructures of choice for the generation of UV light with the shortest wavelengths.[14−17] In contrast to the van der Waals heterostructures based on TMDs, which are still fabricated by the laborious exfoliation technique, such QWs can be grown by molecular beam epitaxy (MBE) with an effective thickness down to one ML. Theoretically, it was shown[17] that the GaN/AlN QWs possess strong quantum confinement in the one-monolayer limit that dramatically enhances the exciton binding energy (up to 230 meV). This allows classification of the GaN/AlN QWs of ML thicknesses as an ultimate 2D system with an extreme quantum confinement of excitons, similar to the ML of TMD. Such a situation is unique for conventional semiconductor heterostructures, where the quantum confinement on the scale of a single ML cannot be usually achieved due to the relatively small contrast in the electronic properties of the well and barrier materials that results in efficient spreading of the wave functions of carriers into the barriers. Nevertheless, no signature of excitonic effects has been detected so far in the ultrathin GaN/AlN QWs, presumably, due to exciton screening by free carriers[17] and a strong inhomogeneous line broadening related to the polarization effects.[18] Thus, the theoretical prediction of the 2D exciton robustness in atomically thin GaN/AlN QWs has not yet been confirmed experimentally. However, it was recently reported that the radiative recombination rate in a 0.6 nm thick Al$_{0.61}$Ga$_{0.39}$N/AlN QW is essentially increased as compared to that obtained

for the 2 nm thick QW, which is suggestive that the confinement enhanced excitonic recombination can compete favorably with the nonradiative one.[19]

Here, we unambiguously demonstrate the excitonic nature of the light emission in the wide temperature range (5−300 K) from the atomically thin single GaN/AlN QWs grown by MBE. We show that such structures can strongly confine charge carriers on the scale of one lattice constant, allowing one to overcome the immanent pyroelectric separation of electrons and holes. This extreme 2D confinement leads to a dramatic increase of the short-range exchange interaction and huge splitting (up to ∼40 meV) between dark and bright excitonic states that is direct evidence of robust excitons. Experimentally, these effects manifest themselves in the radically different kinetics of the emission decay in the ultimately thin (1−2 ML) and relatively thick (3−4 ML) QWs. We explain these effects in the framework of the combined group-theory analysis of the excitonic spectrum and density functional theory (DFT) calculations of the single particle wave functions. Finally, we record for the thinnest 1−2 ML thick QWs an internal quantum yield of the room-temperature excitonic emission as high as ∼75% at the wavelength as short as 235 nm.

We fabricated GaN/AlN heterostructures with the embedded single GaN QWs, whose thicknesses varied from 1 to 5 ML, by plasma-assisted MBE. To ensure the same conditions for photoluminescence (PL) intensity measurements in different samples with the particular GaN thicknesses we used a graded sample where the GaN QW was grown without the substrate holder rotation. In this case, the change of the thickness of the GaN QW was realized just by shifting along the grade direction in one stripe chipped from the sample. In this way, it was possible to greatly minimize or even exclude the intensity difference due to different adjustment of the excitation and detection spots. Structural analysis of the samples was performed using scanning transmission electron microscopy (STEM) studies with an atomic-scale resolution. Typical high-angle annular dark field (HAADF) STEM images are shown in Figure 2. Importantly, the STEM studies were performed on a second (reference) stripe cut adjacent to the preceding one used in the PL experiments. This permitted us to calibrate the average GaN thickness for each sample in a few
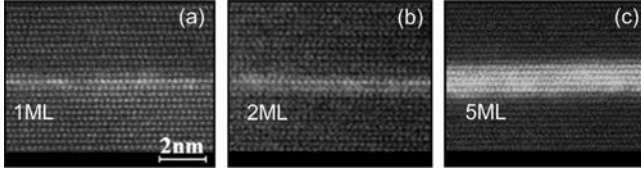
Figure 2. Cross-section STEM images of GaN/AlN structures with intended nominal thicknesses: (a) 1−2 GaN MLs, (b) 2−3 GaN MLs, (c) 4−5 GaN MLs.

selected points along the thickness gradient. In addition, we fabricated a few samples with rotating the substrate holder during growth of the GaN QW. The results obtained with these samples are completely consistent with those obtained with the graded ones. These systematical STEM studies confirmed high reproducibility of the developed technological processes. Details of the growth and characterization of the structures, as well as the optical spectroscopy, are described in the SI.

PL spectra measured in the GaN/AlN structures represent a wide (100−200 meV) inhomogeneously broadened band periodically modulated by light interference fringes in a thick AlN buffer. Characteristic time-integrated spectra are shown in Figure S1a,b. These PL spectra are predominantly TE polarized as confirmed by angular-dependent polarization measurements. With decreasing the GaN thickness, the emission band shifts toward higher energies. Therefore, we attribute the band to the emission of excitons confined in the GaN insertion, whose energy is naturally controlled by the QW thickness. To elucidate the essence of the emission, we performed the PL measurements with time resolution.

Examples of the intensity maps of the time-resolved PL and temperature-dependent decay curves are presented in Figure 3. The most important finding is drastic prolongation of the low-temperature PL decay time, when the GaN thickness decreases down to 1−2 ML.

At low enough temperatures, the 1−3 ML thick QWs demonstrate, in addition, the unusual reversed spectral diffusion of the emission line that is a shift of the line toward higher energies with increasing the delay time after excitation (see Figure S1c,d). This effect is apparently related to the observed increase of the decay time with decreasing the GaN thickness in combination with spatial inhomogeneity of the sample, governed by the GaN thickness fluctuations. Microscopically, these results show that the PL band is due to the emission of localized excitons and that the phonon-assisted hopping of excitons between different localization sites[20,21] is inefficient. Otherwise, it would lead to the usual spectral diffusion: a global shift toward the lower-energy region with increasing delay time. Thus, we assume that the areas of the QW with different effective thicknesses and, hence, different resonance energies are mostly uncoupled (isolated). This intrinsic structure was recently made evident by spreading resistance microscopy, which proved the emergence of an ensemble of disk-shaped GaN islands with a lateral size in the range of tens of nanometers.[22]

In Figure 4a, we present the intensity of the time-integrated and spectrally integrated PL versus temperature. The temperature dependence is strikingly different for the ultimately thin (1 ML, orange line) and thicker (2−3 ML, green and blue lines) QWs (named further as thin and thick QWs, respectively). In the thick QWs emitting light at wavelengths around 250 nm and longer, the PL intensity is independent of
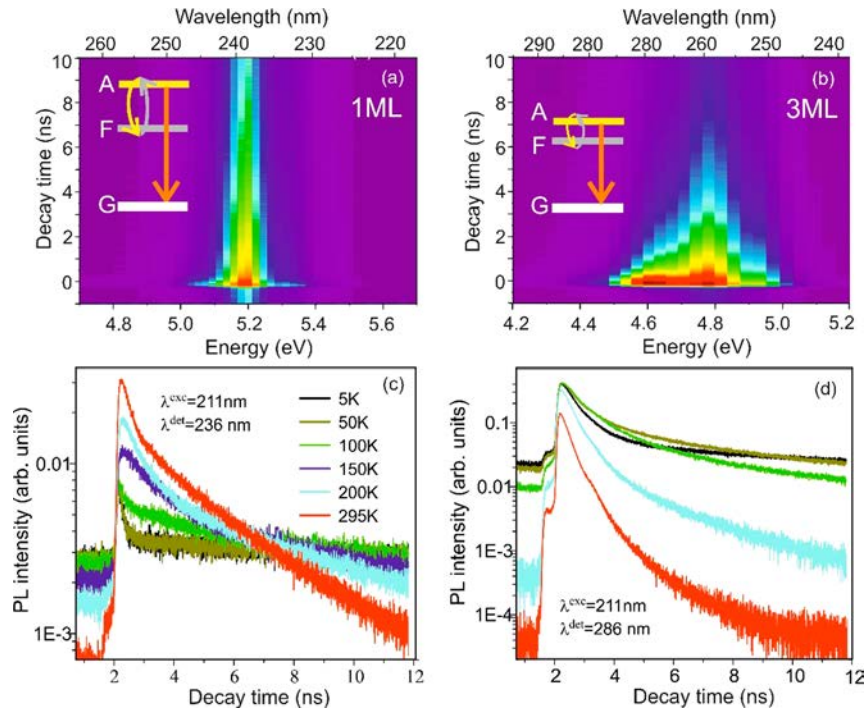
Figure 3. (a, b) Color maps of time-resolved PL intensity (decreasing from red to blue) measured at 77 K in the GaN/AlN structures with the nominal GaN thicknesses (a) 1−2 ML and (b) 2−3 ML. The insets show the schematic of excitonic states where the notations are as follows: A, allowed (bright); F, forbidden (dark); G, ground. (c, d) Selected decay curves of the time-resolved PL measured at different temperatures for (c) 1−2 ML and (d) 2−3 ML thick GaN/AlN QWs. The detection wavelengths are given in the panels and correspond to the centers of gravity of the PL lines. The identical line colors in two plots correspond to the same temperatures.

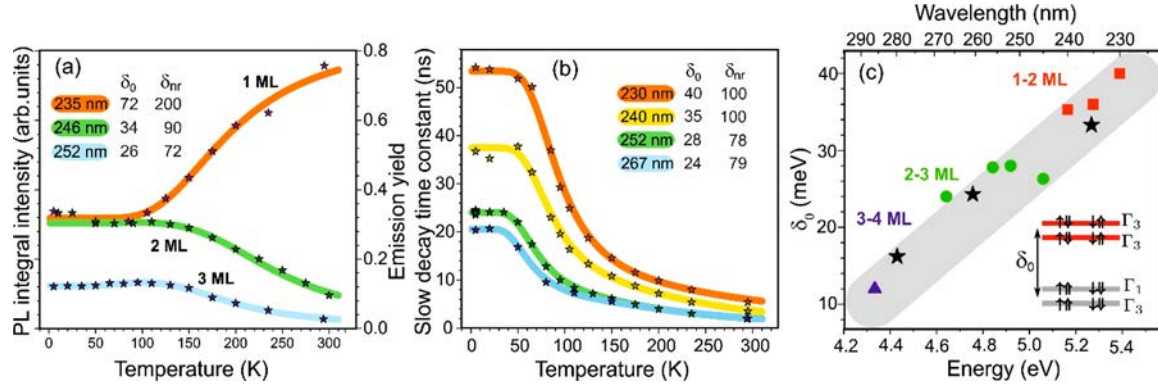**Figure 4.** (a) Temperature dependences of the integral intensities of the emission lines, measured in GaN/AlN QWs of different thicknesses. The wavelengths corresponding to centers of gravity of the lines are given in the legend. The asterisks show experimental data (left axis), and the lines represent the simulations of the internal emission yield (right axis) with the parameters δ_0 and δ_{nr} given in the legend. (b) Representative temperature dependences of the "slow" PL decay time constant. The asterisks are the experimental values registered at different emission wavelengths within the inhomogeneously broadened emission lines in the 1−2 ML thick QWs (230 and 240 nm) and 2−3 ML thick QWs (252 and 267 nm). The solid curves show the theoretical simulations. (c) Energy/wavelength dependence of the exchange splitting δ_0 between the bright−dark excitonic states. Squares, circles, and a triangle represent experimental data for samples attributed to 1−2, 2−3, and 3−4 ML of GaN. Black stars show the fits for these samples based on the DFT calculation with the short-range exchange interaction constant $\varepsilon_0 = 160$ meV. The inset shows the relevant exciton fine structure.

temperature below ∼100 K and steadily decreases above this temperature. This behavior is routine, being usually ascribed to the activated transport of photoexcited carriers toward nonradiative recombination centers.[23] For the thinnest QWs emitting around 235 nm we record an opposite behavior: The PL intensity always increases when the temperature rises from 5 K to ambient. At 300 K, it exceeds the low-temperature intensity by more than 100%. Such temperature dependence suggests the presence of lower-lying, long-living dark states that are preferentially populated at low temperature, whereas the temperature increase gives rise to the thermal activation of higher-lying, short-living bright states (see the insets in Figure 3a,b). As a result, the accelerated rate of radiative decay prevails over the nonradiative one, and the emission yield increases. The samples with an intermediate thickness demonstrate a smooth transition from one type of the temperature dependence to the other. It is obvious that the smaller the energy splitting between these dark and bright states, the stronger the impact of the thermal activation, and the faster the recombination rate. Figure 3a,b illustrates such shortening of the recombination time.

To specify further these two regimes of emission kinetics we focus on the PL decay curves measured in the 1−2 ML (Figure 3c) and 2−3 ML (Figure 3d) thick QWs. In the case of the thick QW, sample heating above ∼100 K results in a steady shortening of an effective decay time, associated with the decrease in the PL integrated intensity, which is again consistent with the temperature-induced activation of non-radiative recombination channels. The PL kinetics in the thin QWs is more complicated and through the whole temperature range is consistent with a model of biexponential decay. The fast decay time constant τ_f at low temperature is less than the temporal resolution of our system (<140 ps). With the increase of the temperature, the fast PL component disappears at $T \sim$ 100 K and then appears again above ∼150 K with longer τ_f of the order of several hundreds of picoseconds. We ascribe the initial fast PL decay at low temperatures to a nonthermalized emission shortly after the optical excitation pulse, like in the ML of TMD.[24] In our case, it is presumably governed by the competition between two processes, namely, the exciton

energy relaxation among bright and dark states and recombination. The slow decay time constant τ_s decreases from tens of ns at low temperatures down to ∼5 ns at room temperature. At the same time, the amplitude of the slow decay component increases with increasing temperature. This again makes evident the temperature activation of the radiative recombination in the thin QW.

It is necessary to underline that the kinetics measurements alone do not allow one to unambiguously determine the nature of the involved dark excitonic states: They can be related either to the large wavevectors outside the light cone or to the spin-forbidden states. In both cases, the relaxation process is governed by interaction with acoustic phonons and can be accompanied by spin flip scattering, whose rate falls within the picosecond and sub-picosecond ranges. However, the temperature behavior of the PL intensity in the QWs of different thicknesses is suggestive of the existence of spin-forbidden states, split from the bright states by an energy gap δ_0 exceeding $k_B T$ for $T = 300$ K. This splitting can be naturally related to the short-range electron−hole spin-exchange interaction,[25,26] whereas its anomalously large value could be caused by the increase of the overlap between electron and hole wave functions in atomically thin QWs. The increase of the temperature activates the population of the higher-lying bright states, which in turn accelerates the exciton decay. To justify and specify the proposed explanation of the emission kinetics we further present theoretical calculations of the electronic states, elaborate the scheme of the fine structure of the excitonic levels (Figure 4c, inset), and model the obtained experimental data.

We perform the DFT calculation of electronic states in atomically thin GaN/AlN QWs, assuming that an ideal wurtzite crystal represents a periodic stacking of cation−anion bilayers (further we consider them as ML) in the direction along the hexagonal c-axis, having infinite size in the lateral directions. Two MLs form a complete period of a wurtzite structure in the [0001] direction. The calculations were performed in the all-electron WIEN2k package as described in the SI. We set the energy convergence to 10^{-5} and charge convergence to 10^{-4} and checked the numerical
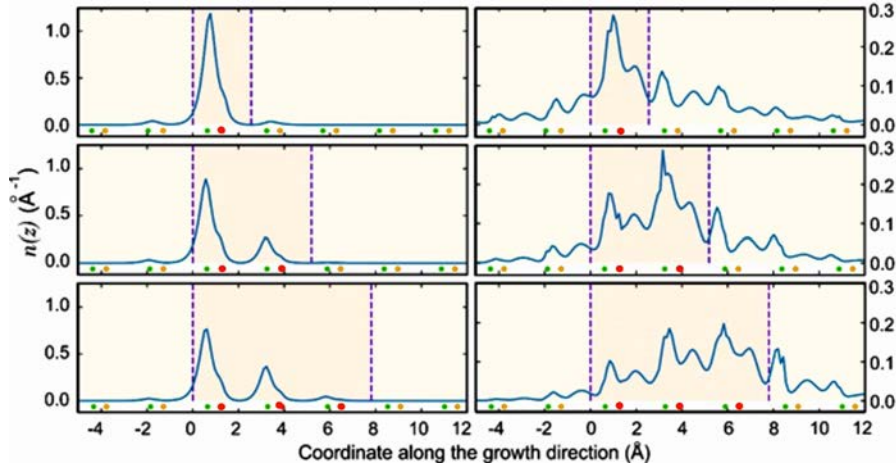
Figure 5. Electron density integrated in the lateral direction in the structure with 1 (top row), 2 (middle row), and 3 (bottom row) ML of GaN within the AlN barriers. The left panels show the first hole level, and the right panels show the first electron level. Color dots show the actual atom projections to the growth direction. Large red dots represent Ga atoms, small green dots N atoms, and yellow dots Al atoms.

accuracy of the calculation by computing the lattice constants and band gaps in bulk GaN and AlN. We find that the lattice constants agree with the experimental values within 1% error. The band gap in this scheme is underestimated for GaN by about 7% and for AlN by about 20%, which is reasonable for the qualitative analysis. Figure 5 shows the wave functions of the ground hole (left panels) and electron (right panels) states, obtained in the framework of the DFT for an AlN wurtzite crystal with one, two, and three atomic layers of Al being replaced by an atomic layer of Ga.

In a 1 ML QW, the ground hole density is pinned to the atomic layer of nitrogen anions adjacent to the atomic layer of Ga cations. The electron state concentrates around the same nitrogen atoms, but noticeably spreads toward the "metal-face" direction. The asymmetry of the distribution is caused by the spontaneous and piezoelectric polarizations, which results in a built-in electric field.[18] It is important to emphasize that both electron and hole states are strongly confined within one lattice constant (two ML) around the GaN QW. Thanks to this extreme thinness, their overlap is strong despite the pyro-electric nature of the involved materials. This situation changes dramatically with an increase of the GaN thickness. The electron state becomes more evenly distributed across the insertion, whereas the hole state remains pinned to the nitrogen atomic layer from the "Ga-face" side. As a result, the overlap of the electron and hole wave functions decreases a few times with increasing the QW thickness by only 1−2 ML. The modeling makes evident a fast and steady decrease of the oscillator strength of the interband optical transitions with an increase of the GaN thickness. This means the increase of the intrinsic radiative lifetime with the decrease of the transition energy.

Remarkably, the experimental observation is quite opposite to the theoretical modeling based on the single-particle calculations. Namely, the higher the emission energy, the longer the observed PL lifetime. This behavior, however, can be readily described provided excitonic origin of the emission. The decrease of the QW width leads to the enhancement of the splitting between dark and bright exciton states due to the enhanced exchange interaction, which increases the average exciton lifetime. Besides the quantum confinement along the growth direction, one should also consider in-plane exciton

localization due to the fluctuation of the QW thickness between the islands. In this case, the exciton energy is additionally affected by the lateral size of the localization area. In the QW plane, the exciton Bohr radius is less than 1 nm; thus, the exciton can be quantized in a slowly varying 2D potential as a whole. For the lateral exciton localization, this results in the higher exciton energy and, respectively, in a longer lifetime because of the admixture of the large-wavevector components in the exciton wave function.[27]

Now, let us describe the fine structure of the excitonic levels in the ultrathin GaN QWs. Note that in the bulk GaN the exchange interaction between electron and hole in an exciton is less than 1.0 meV[28,29] and cannot change the exciton kinetics at room temperature. The dramatic enhancement of the short-range exchange interaction in atomically thin QWs is caused by the extreme confinement of electron and hole along the growth axis and an order of magnitude decrease of the exciton Bohr radius. The latter is contributed by the 2D confinement, an increase of the effective masses,[17] and reduction of the dielectric screening by optical phonons. In total, the electron−hole exchange interaction can increase by 2−3 orders of magnitude in the atomically thin QWs, as compared to the bulk crystal.

The extreme confinement also leads to the qualitative change of the Bloch wave functions in the valence band. The calculations show that in the ground hole state the splitting between the spin doublet originating from p_z orbitals and the states originating from p_x and p_y orbitals is strongly enhanced (up to a few hundreds of meV). As a result, the fine structure of lowest excitonic levels consists of 8 states (see the detailed description of the group-theory analysis in the SI). The four lowest states are dark, and the four upper states are bright. The splitting between these states δ_0 is determined by the giant short-range exchange interaction. Each group of states additionally splits into two doublets by the spin−orbit interaction, as shown in the inset in Figure 4c. The lowest doublet of the dark states transforms under Γ_3 representation of C_{3v} group; the next pair is degenerate neglecting the interaction with the remote bands and transforms under $\Gamma_1 \oplus \Gamma_2$ representations. Both pairs of the bright states belong to Γ_3 representation and have in-plane dipole moments needed for radiative recombination.

Elucidation of the exciton fine structure allows us to describe quantitatively the temperature dependence of the PL decay and internal quantum yield (detailed description of the procedure and obtained results are given in the SI). At a given temperature, the effective radiative decay time in a 2D structure like a QW reads as[6]

$$\tau_{\text{rad}}^{\text{eff}} = \frac{3}{2}\frac{k_B T}{E_0}\tau_{\text{rad}}^0 \tag{1}$$

where $\tau_{\text{rad}}^0 = \frac{1}{2\Gamma_0}$ is the low-temperature radiative lifetime at the in-plane exciton wave-vector $k_\parallel = 0$, Γ_0 is the respective decay rate, and E_0 represents the above-discussed radiative window.

For the thermalized emission the effective radiative decay rate τ_{eff} is given by the average of the decay rates of different excitonic levels

$$\langle\tau_{\text{eff}}\rangle^{-1} = \frac{\sum_i \langle\tau_i\rangle^{-1} e^{-E_i(0)/k_B T}}{\sum_i e^{-E_i(0)/k_B T}} \tag{2}$$

Here, the average radiative lifetimes of an exciton $\langle\tau_i\rangle$ in a state i at temperature T are the fitting parameters. For bright excitons, $\langle\tau_b\rangle$ is governed by the intrinsic radiative exciton lifetime τ_{rad}^0, the optical window width E_0, and temperature T. For the spin-forbidden dark excitons, $\langle\tau_d\rangle$ should be much longer, since the related emission is due, most probably, to intersite hopping, phonon- and impurity-assisted processes, and states mixing (see the SI for details). To simplify the fitting procedure, we set decay times equal within the two groups of both bright (τ_b) and dark (τ_d) excitons. Their characteristic values at low temperature and the energy splitting between the bright and dark exciton states δ_0 are assumed as principal fitting parameters. In addition, we phenomenologically introduce an extra level shifted in energy by δ_{nr}, which is responsible for the thermally activated nonradiative recombination, characterized by τ_{nr}.[30] Previously, a similar approach was successfully employed to simulate the exciton recombination kinetics in both carbon nanotubes[31] and 2D crystals of TMDs.[32]

Experimentally, the equilibrium emission kinetics is characterized by the decay time constant τ_s, corresponding to the slowest stage of the PL decay, extracted within a biexponential model from the decay curves measured at different temperatures (like those in Figure 3c,d). These data are fitted as

$$\frac{1}{\tau_s(T)} = \frac{1}{\tau_{\text{eff}}(T)} + \frac{1}{\tau_{\text{nr}}(T)} \tag{3}$$

The solid lines in Figure 4b show the fits of the slow time τ_s as a function of temperature, obtained for the values of the parameters δ_0 and δ_{nr} given in the plot legend. For the thinnest (~1 ML) GaN QW emitting around 235 nm, δ_0 is comparable with the $k_B T$ at 300 K, whereas $\delta_{\text{nr}} = 100$ meV is much larger, which indicates the nearly constant rate of the nonradiative decay Γ_{nr} in the temperature range from 5 to 300 K. This observation is consistent with the assumed discontinuous structure of the single GaN ML, preventing the thermally activated in-plane transport of photoexcited carriers toward centers of nonradiative recombination. By contrast, for the QWs thicker than 2−3 ML, the smaller decay time constant at elevated temperatures is determined by the nonradiative recombination that implies smaller activation energy of the in-plane transport of charge carriers along the QW and the

enhanced effect of spontaneous polarization, which leads to exciton dissociation and, respectively, to faster electron−hole recombination. From Figure 4a we can roughly estimate the emission wavelength separating these two regimes as ~240 nm, which corresponds to the emission of a ~2 ML thick GaN/AlN QW.

The splitting parameter δ_0 extracted from the fit of experimental data for different samples as a function of the emission wavelength is shown in Figure 4c. The points in the plot perfectly comply with a monotonic dependence, thus demonstrating a continuous increase of δ_0 from ~10 meV for the ~4 ML thick insertions up to ~42 meV for the thinnest (~1 ML) insertion. From the comparison of experimental values of δ_0 and the calculations of the wave functions we estimate the short-range exchange interaction constant in GaN as $\varepsilon_0 = 160$ meV that is consistent with published data (see the SI). Recently, in ref 33, the quantum confinement energy and exciton exchange splitting in atomically thin GaN QWs embedded in AlN have been obtained by the sophisticated first-principle calculations. For 1 ML, the calculated band gap energy is in perfect agreement with our experimental data, while the calculated exchange splitting is approximately 2 times smaller than the experimental value.

The internal quantum efficiency is frequently estimated as a ratio of the light emission intensities at room temperature and low temperature.[34] This method is based on the assumption that at the lowest temperatures the nonradiative recombination Γ_{nr} is much slower than the radiative one (Γ_r), because any diffusion of photoexcited carriers is suppressed, and the internal emission yield $Y = \Gamma_r/(\Gamma_r + \Gamma_{\text{nr}})$ is nearly 100%. In the case of the 1−2 ML thick GaN QW, this method is obviously incorrect. The low-temperature emission process in this structure is mainly relevant to dark excitonic states whose radiative decay $\tau_{\text{d,r}}$ is very long (infinitely long for the completely forbidden excitons), and even vanishingly small nonradiative decay $\tau_{\text{d,nr}}$ can result in a noticeable deviation of the internal quantum efficiency from 100%. In these conditions, the decay constant τ_d can be expressed as $\frac{1}{\tau_d} = \frac{1}{\tau_{\text{d,r}}} + \frac{1}{\tau_{\text{d,nr}}}$ where both $\tau_{\text{d,r}}$ and $\tau_{\text{d,nr}}$ should be longer than τ_d. The experimentally observed steady increase of the PL intensity with temperature confirms this assumption (see Figure 4a). Thus, any theoretical simulation of the emission intensity versus temperature, aimed at elucidation of the internal emission efficiency, should consider the nonradiative contribution at all temperatures, however small it is.

To perform such a simulation, we consider the experimental data on the emission intensity (Figure 4a) and the slow PL decay time (Figure 4b) simultaneously. The integration of the decay curves shown in Figure 3c confirms the negligibly small contribution of nonthermalized PL at any temperature. In this case, the PL integral intensity is directly proportional to the internal emission yield, and we can perform, provided that the emission is purely excitonic, even quantitative estimation of this parameter as a function of temperature. At the lowest temperatures (below ~100 K), the emission yield is governed by the residual radiative decay $\tau_{\text{d,r}}$, which is relevant to dark excitons alone, since the bright excitonic states are not populated. This radiative decay, while being weak, provides the entire registered PL signal. The enhanced temperature results in an increase in the emission yield that is possible only if Γ_{nr} is nonzero. The proportionality coefficient between the measured

PL intensities and the internal emission yield reflects the output efficiency of the emission (see the SI for details).

Such modeling of the experimentally measured integrated PL intensity versus temperature allows the estimation of the internal quantum yield in an absolute scale (see the scale of the right axis in Figure 4a). For the thinnest GaN insertion at 300 K, the yield value is as large as ∼75%. The corresponding decay parameters at low temperature are τ_d = 45 ns, $\tau_{d,r}$ = 140 ns, and $\tau_{d,nr}$ = 66 ns. Thus, a nonradiative decay channel is dominating in the QW emission at the lowest temperatures, whereas further thermal activation of the bright excitonic states gives rise to the enhanced both radiative decay and internal emission yield.

The experimental data presented in Figure 4a,b show that the same model is able to describe consistently the whole set of experimental data, while the parameters obtained by fitting either the emission yield or the slow decay time constant versus temperature are somewhat different. This is not surprising since the integral intensity in Figure 4a is averaged over the inhomogeneous PL line, whereas the values of τ_s in Figure 4b are related to selected wavelengths. Nevertheless, our estimations prove reliably that only the atomically thin GaN/AlN QWs with extreme 2D confinement are suitable for the efficient room-temperature excitonic emission in the deep-UV spectral range.

In summary, we demonstrated a giant enhancement of the short-range electron−hole spin-exchange in atomically thin GaN/AlN QWs that is a firm signature of the 2D exciton nature of light emission in the 1−2 ML thick QWs at temperatures up to 300 K. The strongly confined exciton is of paramount importance for designing efficient UV light-emitting devices with a possibly short emission wavelength. Owing to the suppressed nonradiative recombination and short intrinsic radiative lifetime of the 2D excitons, we obtained a record room-temperature internal quantum efficiency which is about 75% at wavelengths around 235 nm.

AUTHOR INFORMATION

Corresponding Author
*E-mail: toropov@beam.ioffe.ru.

ORCID ◉
A. A. Toropov: 0000-0002-5712-8350
M. O. Nestoklon: 0000-0002-0454-342X
T. V. Shubina: 0000-0003-1092-8382
V. N. Jmerik: 0000-0001-8759-7273

Author Contributions
The sample growth was done by V.N.J. and D.V.N. TEM characterization was performed by S.R. Optical experiments were carried out by E.A.E., V.K.K., T.V.S., and A.A.T. Theoretical calculations were done by M.O.N., G.V.B., and D.S.S. Optical data modeling was performed by E.A.E. and A.A.T. The paper was written by A.A.T., T.V.S., M.O.N., and D.S.S. All authors discussed the results and commented on the manuscript at all stages. This work was supervised by S.V.I. and B.G.

REFERENCES

(1) Ivchenko, E. L. *Optical spectroscopy of semiconductor nanostructures*; Alpha Science: Harrow, UK, 2005.
(2) Weisbuch, C.; Miller, R. C.; Dingle, R.; Gossard, A. C.; Wiegmann, W. *Solid State Commun.* **1981**, 37, 219−222.
(3) Deveaud, B.; Clérot, F.; Roy, N.; Satzke, K.; Sermage, B.; Katzer, D. S. *Phys. Rev. Lett.* **1991**, 67, 2355−2358.
(4) Mak, K. F.; Lee, C.; Hone, J.; Shan, J.; Heinz, T. F. *Phys. Rev. Lett.* **2010**, 105, 136805.
(5) Wang, G.; Chernikov, A.; Glazov, M. M.; Heinz, T. F.; Marie, X.; Amand, T.; Urbaszek, B. *Rev. Mod. Phys.* **2018**, 90, No. 021001.
(6) Andreani, L. C.; Tassone, F.; Bassani, F. *Solid State Commun.* **1991**, 77, 641−645.
(7) Rinke, P.; Winkelnkemper, M.; Qteish, A.; Bimberg, D.; Neugebauer, J.; Scheffler, M. *Phys. Rev. B: Condens. Matter Mater. Phys.* **2008**, 77, No. 075202.
(8) Robert, C.; Lagarde, D.; Cadiz, F.; Wang, G.; Lassagne, B.; Amand, T.; Balocchi, A.; Renucci, P.; Tongay, S.; Urbaszek, B.; Marie, X. *Phys. Rev. B: Condens. Matter Mater. Phys.* **2016**, 93, 205423.
(9) Kneissl, M.; Rass, J. *III-Nitride Ultraviolet Emitters: Technology and Applications*; Springer Series in Materials Science; Springer: New York, 2016; Vol. 227.
(10) Islam, S. M.; Lee, K.; Verma, J.; Protasenko, V.; Rouvimov, S.; Bharadwaj, S.; Xing, H.; Jena, D. *Appl. Phys. Lett.* **2017**, 110, No. 041108.
(11) Rong, X.; Wang, X.; Ivanov, S. V.; Jiang, X.; Chen, G.; Wang, P.; Wang, W.; He, C.; Wang, T.; Schulz, T.; Albrecht, M.; Jmerik, V. N.; Toropov, A. A.; Ratnikov, V. V.; Kozlovsky, V. I.; Martovitsky, V. P.; Jin, P.; Xu, F.; Yang, X.; Qin, Z.; Ge, W.; Shi, J.; Shen, B. *Adv. Mater.* **2016**, 28, 7978−7983.
(12) Jmerik, V. N.; Nechaev, D. V.; Toropov, A. A.; Evropeitsev, E. A.; Kozlovsky, V. I.; Martovitsky, V. P.; Rouvimov, S.; Ivanov, S. V. *Appl. Phys. Express* **2018**, 11, No. 091003.
(13) Wood, C.; Jena, D. *Polarization effects in semiconductors from ab initio theory to device applications*; Springer: New York, 2008.
(14) Furis, M.; Cartwright, A. N.; Wu, H.; Schaff, W. J. *Appl. Phys. Lett.* **2003**, 83, 3486.
(15) Kamiya, K.; Ebihara, Y.; Shiraishi, K.; Kasu, M. *Appl. Phys. Lett.* **2011**, 99, 151108.
(16) Taniyasu, Y.; Kasu, M. *Appl. Phys. Lett.* **2011**, 99, 251112.
(17) Bayerl, D.; Islam, S. M.; Jones, C. M.; Protasenko, V.; Jena, D.; Kioupakis, E. *Appl. Phys. Lett.* **2016**, 109, 241102.
(18) Deguchi, T.; Sekiguchi, K.; Nakamura, A.; Sota, T.; Matsuo, R.; Chichibu, S.; Nakamura, S. *Jpn. J. Appl. Phys.* **1999**, 38, L914.
(19) Haughn, C. R.; Rupper, G.; Wunderer, T.; Yang, Z.; Johnson, N. M.; Wraback, M.; Garrett, G. A. *Appl. Phys. Lett.* **2019**, 114, 102101.
(20) Takagahara, T. *J. Lumin.* **1989**, 44, 347−366.

(21) Kalt, H.; Collet, J.; Baranovskii, S. D.; Saleh, R.; Thomas, P.; Dang, Le Si; Cibert, J. *Phys. Rev. B: Condens. Matter Mater. Phys.* **1992**, *45*, 4253−4257.

(22) Sviridov, D. E.; Jmerik, V. N.; Rouvimov, S.; Nechaev, D. V.; Kozlovsky, V. I.; Ivanov, S. V. *Appl. Phys. Lett.* **2019**, *114*, No. 061601.

(23) Chichibu, S. F.; Uedono, A.; Onuma, T.; Haskell, B. A.; Chakraborty, A.; Koyama, T.; Fini, P. T.; Keller, S.; DenBaars, S. P.; Speck, J. S.; Mishra, U. K.; Nakamura, S.; Yamaguchi, S.; Kamiyama, S.; Amano, H.; Akasaki, I.; Han, J.; Sota, T. *Nat. Mater.* **2006**, *5*, 810−816.

(24) Zhang, X. X.; You, Y.; Zhao, S. Y. F.; Heinz, T. F. *Phys. Rev. Lett.* **2015**, *115*, 257403.

(25) Monemar, B.; Paskov, P. P.; Bergman, J. P.; Toropov, A. A.; Shubina, T. V.; Malinauskas, T.; Usui, A. *Phys. Status Solidi B* **2008**, *245*, 1723−1740.

(26) Chen, Y.; Gil, B.; Lefebvre, P.; Mathieu, H. *Phys. Rev. B: Condens. Matter Mater. Phys.* **1988**, *37*, 6429.

(27) Citrin, D. S. *Phys. Rev. B: Condens. Matter Mater. Phys.* **1993**, *47*, 3832.

(28) Julier, M.; Campo, J.; Gil, B.; Lascaray, J. P.; Nakamura, S. *Phys. Rev. B: Condens. Matter Mater. Phys.* **1998**, *57*, R6791.

(29) Paskov, P. P.; Paskova, T.; Holtz, P. O.; Monemar, B. *Phys. Rev. B: Condens. Matter Mater. Phys.* **2001**, *64*, 115201.

(30) Neogi, A.; Morkoç, H.; Kuroda, T.; Tackeuchi, A.; Kawazoe, T.; Ohtsu, M. *Nano Lett.* **2005**, *5*, 213−7.

(31) Spataru, C. D.; Ismail-Beigi, S.; Capaz, R. B.; Louie, S. G. *Phys. Rev. Lett.* **2005**, *95*, 247402.

(32) Palummo, M.; Bernardi, M.; Grossman, J. C. *Nano Lett.* **2015**, *15*, 2794.

(33) Bayerl, D.; Kioupakis, E. *Appl. Phys. Lett.* **2019**, *115*, 131101.

(34) Gurioli, M.; Vinattieri, A.; Colocci, M.; Deparis, C.; Massies, J.; Neu, G.; Bosacchi, A.; Franchi, S. *Phys. Rev. B: Condens. Matter Mater. Phys.* **1991**, *44*, 3115.